

20 **Abstract**

21 Air-water CO₂ fluxes in estuarine environments are characterized by high interannual
22 variability, in part due to hydrological variability that alters estuarine carbonate chemistry
23 through multiple physical and biogeochemical processes. To understand the relative
24 contributions of these varied controls on interannual air-water CO₂ fluxes in the mainstem
25 Chesapeake Bay, we implemented both hindcast and scenario simulations using a coupled
26 physical-biogeochemical model. Significant spatiotemporal variability in bay-wide fluxes was
27 found over a 10-year period (1996-2005), where the mainstem Bay was primarily a net CO₂
28 sink, except in drought periods. Sensitivity scenario results suggested substantial effects of
29 riverine nutrient and organic matter (OM) inputs to CO₂ flux variations. The high correlations
30 between riverine inputs and upper-Bay fluxes were due to elevated respiration under increased
31 OM inputs. The interannual flux variations in the lower Bay was mostly regulated by the
32 nutrient inputs. Both nutrient and OM inputs contributed to the flux variability in the mid Bay.
33 It is found that the interannual CO₂ flux of the mainstem was most sensitive to riverine nutrient
34 inputs associated with the hydrological changes. For each hindcast simulation we computed
35 the ratio of organic carbon turnover time to water residence time (λ), a proxy for CO₂ efflux
36 potential, and found that the wetter periods had a relatively lower λ . The variability of
37 mainstem CO₂ fluxes can be well represented using a generic function of λ . The model results
38 showed that higher river flows would lead to enhanced CO₂ sinks into a large eutrophic estuary
39 by promoting net autotrophy.

40

41

42 **Keyword:** CO₂ flux, hydrological effects, the Chesapeake Bay, numerical modelling,
43 interannual variability.

44

45 **1. Introduction**

46 Estuarine CO₂ fluxes represent an important part of the global carbon budget. The total CO₂
47 degassing from estuaries has been estimated to balance the CO₂ uptake from the entire
48 continental shelf, although the estuarine surface area equates to only 0.3% of the oceans and
49 continental shelves (Cai et al., 2011; Borges et al., 2005). Estuaries are biogeochemically active
50 areas that connect terrestrial, riverine, oceanic and atmospheric carbon cycling, and air-water
51 CO₂ exchanges in estuaries are influenced by varying and complex physical, biological and
52 chemical processes, displaying large spatial and temporal variations (Abril & Borges, 2005;
53 Regnier et al., 2013; Gypens et al., 2009). Hence, estimates of CO₂ fluxes in estuarine
54 environments often have high variability in magnitude and direction, and the underlying
55 mechanisms in controlling CO₂ exchanges are not fully understood yet. Small, river-dominated,
56 and anthropogenically impacted estuarine systems worldwide generally show significant
57 heterotrophy, and are primarily strong CO₂ sources to the atmosphere (Caffrey, 2004; Laruelle
58 et al., 2010; Cai and Wang, 1998). Unlike small systems, limited studies in large estuaries
59 implied that large estuarine systems are often high in primary production, and mostly act as
60 weak CO₂ sources or net sinks, such as the Guanabara Bay (Cotovicz et al., 2015), the
61 Chesapeake Bay (Chen et al., 2020; Herrmann et al., 2020; Li et al., 2023), the Delaware Bay
62 (Joesoef et al., 2015, 2017), and the St. Lawrence Estuary (Dinauer and Mucci, 2017).

63 River flows play an important and complex role in regulating carbonate chemistry and
64 air-water CO₂ exchanges in estuarine environments with competing effects (Yao et al., 2020;
65 Pacheco et al., 2015). Organic matter (OM) and nutrient inputs from surrounding tributaries
66 could vary significantly between dry and wet periods. Riverine OM inputs could increase
67 estuarine respiration, therefore elevating water column *p*CO₂ and promoting CO₂ efflux to the
68 atmosphere (Rosentreter et al., 2018; Xiao et al., 2020). In contrast, elevated freshwater inflow
69 delivers more nutrients to estuaries and subsequently enhances autotrophic production and
70 increases CO₂ influx (Shen et al., 2019a; Zhong et al., 2021). River flows may also affect the
71 riverine-estuarine mixing and water residence time, both of which would greatly influence the
72 estuarine CO₂ exchanges (Van Dam et al., 2018; Crosswell et al., 2012; Jiang et al., 2008).

73 Riverine waters are generally high in $p\text{CO}_2$ (i.e., supersaturation condition), and the extensive
74 riverine mixing during high-flow years would strengthen the net CO_2 efflux, particularly in
75 regions closer to freshwater input locations. Estuaries with long water residence times may
76 retain more dissolved inorganic carbon (DIC) generated from oxidation of autochthonous and
77 allochthonous organic matter, and the enriched DIC is most likely released to the atmosphere
78 rather than exported to the coastal regions (Joesoef et al., 2017; Borges & Abril, 2011).

79 Increasing efforts have been made in recent years to understand inorganic carbon cycling
80 and CO_2 fluxes in Chesapeake Bay, and the diversity of reported results highlights the
81 underlying variability in CO_2 fluxes. Chen et al. (2020) reported the first bay-wide,
82 annual-scale observations of air-water CO_2 fluxes along the mainstem, and concluded that the
83 Bay was a weak CO_2 source during the dry hydrological year 2016. Simulations using
84 process-based models suggested the Chesapeake Bay as a whole was a net CO_2 sink, despite the
85 significant spatiotemporal heterogeneity in bay-wide CO_2 fluxes (St-Laurent et al., 2020; Shen
86 et al., 2019a). Because Chesapeake Bay is a larger (~320 km) system, it includes low-salinity
87 and heterotrophic upper reaches that are net CO_2 sources, and high-salinity and
88 nutrient-enriched lower regions that are CO_2 sinks. The Chesapeake Bay's drainage basin is
89 particularly large, and more than 150 major rivers and streams flow into the Bay through a
90 subset of larger tributary rivers. The variability of tributary inflows over a dry-wet cycle would
91 inevitably alter bay-wide biogeochemical cycling and the CO_2 flux. Herrmann et al. (2020)
92 calculated long-term (1998-2018) CO_2 fluxes of the mainstem Bay based on historical water
93 quality data, indicating the mainstem was a weak CO_2 source to the atmosphere and the high
94 CO_2 effluxes were mostly related to high bay-wide salinity (i.e., relatively low streamflow
95 conditions). Thus, it is still challenging to separate and distinguish the effects of multiple
96 factors (e.g., nutrient and OM inputs, riverine mixing) associated with hydrological conditions
97 in different years on air-water exchanges in diverse estuaries, despite the need to better quantify
98 these rates to understand the role of estuaries in the global carbon cycle.

99 The goal of this study is to explore the hydrological controls on air-water CO_2 fluxes in the
100 mainstem Chesapeake Bay. The Chesapeake Bay is an ideal system within which to conduct

101 this study, given its diversity of physical and chemical environments over which to quantify
102 CO₂ fluxes in response to riverine inputs. We used a well-calibrated, coupled
103 physical-biogeochemical model to examine the spatiotemporal variability of CO₂ chemistry
104 and the annual CO₂ flux in the mainstem over a 10-year period (1996-2005) with a changing
105 hydrological regime (i.e., dry-wet cycles). Experimental scenarios were designed, and
106 sensitivity simulations were conducted to isolate the physical (mixing, input) versus biological
107 (nutrient-induced productivity and respiration of OM inputs) factors associated with the
108 hydrological cycles in regulating the air-water CO₂ flux.

109

110 **2. Materials and methods**

111 **2.1. Study site**

112 The Chesapeake Bay, located in the United States mid-Atlantic coastal region, is the
113 largest estuary in the United States and drains approximately 168,000 km² of watershed from
114 the states of Maryland, Virginia, New York, Delaware, West Virginia, Pennsylvania, and the
115 District of Columbia. The mainstem Bay is approximately 320 km long from the northern
116 Susquehanna River to its southern mouth in the Atlantic Ocean (Fig. 1). The average depth is
117 6.5 m and a relatively deep central channel (20–35 m) runs the length of the middle region of
118 the Bay. Water circulation in the mainstem is a typical two-layer pattern, consisting of the
119 seaward movement of freshwater from the north and bottom intrusion of seawater from the
120 south (Li et al., 2005). The water residence time of Chesapeake Bay was estimated in a range of
121 110 to 264 days, with an average of 180 days (Du & Shen, 2016). The Susquehanna River,
122 among the major tributaries (Fig. 1) including the Potomac, James and York Rivers, is the
123 largest tributary draining the watershed. It provides ~90% of the freshwater flow to the upper
124 Bay and ~60% of the freshwaters to the entire mainstem, and is the only tributary that drains
125 directly into the mainstem of Chesapeake Bay. Tributary inflows in Chesapeake Bay
126 watersheds show clear seasonal and interannual variations. The annual freshwater inflows from
127 tributaries into the Bay could reach 3000 m³ s⁻¹ in high-flow wet years, but only 1000 m³ s⁻¹ in
128 dry years. We divided the mainstem into three regions to explore the spatial variability in CO₂

129 fluxes: upper Bay (north of 38.6° N), mid Bay (between 37.6° and 38.6° N) and lower Bay
130 (south of 37.6° N) following Magnuson et al. (2004, Fig. 1) with a transition from freshwater to
131 the ocean. The upper and lower Bay are freshwater-dominated and ocean-dominated regions,
132 respectively, and the mid Bay is a mixture of the two.

133

134 **2.2. Physical-Biogeochemical model**

135 A three-dimensional physical-biogeochemical model (ROMS-RCA-CC) was used to
136 explore the hydrological controls on CO₂ fluxes of the mainstem Chesapeake Bay. The coupled
137 biophysical model has been well validated and applied in Chesapeake Bay to explore the
138 interactions among physical, biological and chemical processes. In particular, the coupled
139 model includes a physical Regional Ocean Modelling System (ROMS) configured for
140 Chesapeake Bay (Li et al., 2005), a water quality model, Row Column Aesop (RCA),
141 simulating variable forms (e.g., inorganic and organic, dissolved and particulate) of carbon,
142 nitrogen, phosphorus and phytoplankton, DO in both the water column and sediments (Testa
143 et al., 2014), and a carbonate chemistry (CC) module tracking key state variables of carbonate
144 chemistry including DIC, total alkalinity (TA), pH and *p*CO₂ (Shen et al., 2019a; Li et al.,
145 2020, 2023). The model mesh grid is 80×120 cells with ~1 km width (Fig. 1), and the time step
146 for the biogeochemical model is 5 min to ensure a high spatiotemporal resolution for this study.
147 The model adopts the sigma coordinate system in the vertical direction and is set up with 20
148 layers uniformly. A detailed description of the biogeochemical model configuration (e.g., the
149 boundary forcing, simulation performances) and validation can be found in the supplemental
150 material. The schematic diagram of the major state variables and transformation process in
151 RCA-CC is presented in Fig. S1.

152 Air-water CO₂ exchanges were calculated as a function of transfer velocity, solubility and
153 the *p*CO₂ difference between surface water and the air (Eq. 1).

$$154 \quad F = v \times K \times (pC_{a, r} - pC_{w, ter}) \quad (1)$$

155 where *K* is the solubility of CO₂ from Weiss (1974), *p*C_{*a, r*} is the atmospheric CO₂ partial
156 pressure, and *v* is the gas transfer velocity from Wanninkhof (2014),

157
$$v = 0.251 \times u_{10} \sqrt{\frac{660}{S}} \quad (2)$$

158 In Eq. 2, v has units of cm hr^{-1} , u_{10} is the 10-m height wind speed in m s^{-1} , which is measured
159 at the Patuxent River Naval Air Station (KNHK, 38.5N, 76.7W), and Sc is the
160 temperature-dependent Schmidt number. A positive flux from our calculation represents CO_2
161 release to the atmosphere or efflux, while a negative value represents CO_2 uptake by the water
162 side or influx. Air-water CO_2 fluxes at each mesh grid in a year were added together, then
163 divided by the total area of different regions to obtain the area-weight means. Atmospheric
164 $p\text{CO}_2$ has been measured with an increase of 1.8 ppm each year due to continuous
165 anthropogenic carbon emissions. As we focused on the impacts of river flows on interannual
166 CO_2 fluxes in this study, we used a constant atmospheric $p\text{CO}_2$ between 1996-2005 to remove
167 flux variations resulted from the increasing CO_2 levels in the air (i.e., 370 ppm measured at the
168 Mauna Loa Observatory in year 2000, (<https://gml.noaa.gov/ccgg/trends/>). Given that the
169 variability in water $p\text{CO}_2$ is much greater than this small air $p\text{CO}_2$ increase, this approach will
170 not affect the results.

171

172 **2.3. Model experiments**

173 A control simulation was conducted to represent a 10-year period from January 1996 to
174 December 2005, incorporating realistic riverine inputs (e.g., nutrient and OM loading, tributary
175 discharges), coastal open boundary and meteorological forcing (e.g., tides, wind speed,
176 shortwave radiation). The 10-year period (1996-2005) was chosen for this study, as it contains
177 years with varying hydrological conditions (Fig. 2), including dry (1999, 2000, 2001, 25%
178 more inflow than the average during 1986-2020), wet (1996, 2003, 2004, 25% less inflow than
179 the average) and normal (1998) years. In addition, the coupled physical-biogeochemical model
180 has been sufficiently validated in Chesapeake Bay for these 10 years from perspectives of
181 physical advection and mixing (Li et al., 2005), nutrient and DO cycling (Testa et al., 2014; Li
182 et al., 2016; Ni et al., 2020), and bay-wide variability of carbonate chemistry (Shen et al.,
183 2019b, 2020).

184 The control simulation (Control) was compared to the results of two sensitivity scenarios in
185 order to evaluate the relative impacts of riverine discharges on air-water CO₂ exchanges in the
186 mainstem Bay. The dry-wet cycles would significantly change the nutrient and OM inputs from
187 incoming rivers, therefore altering primary production/respiration and air-water CO₂ fluxes. In
188 one experimental scenario, we applied an annually-constant nutrient loading from the
189 Susquehanna River (RiverN) over the 10-year period. Specifically, the annually averaged
190 inorganic nitrogen (including NO₂⁻, NO₃⁻, NH₄⁺) loading was calculated, and we
191 decreased/increased the riverine concentrations of inorganic nitrogen for each year, but keeping
192 the freshwater discharge the same, to obtain a constant nitrogen loading for the study period
193 (Fig. S2, e.g., the N concentrations were reduced in wet years, but increased in dry years.). To
194 quantify the relative impacts of riverine OM loading (DOC and POC loading only), a set of
195 riverine dissolved organic carbon (DOC) and particulate organic carbon (POC) experiments
196 (RiverC) was conducted (Fig. S2). Similarly, these included increasing/decreasing the riverine
197 organic carbon concentrations to remove the interannual variability in OM loading from the
198 Susquehanna River. Model configurations including the impacts of CDOM and TSS on the
199 light attenuation coefficient K_d and sinking velocity were not modeled to dynamically respond
200 to riverine loading in the scenario model runs, although the time and space-varying impacts of
201 TSS and CDOM on K_d values in the control run were included based on observational data
202 (Testa et al. 2014). Both these two scenario experiments were run over the 10-year period, and
203 compared with the control experiments.

204

205 **3. Results**

206 **3.1. Control simulations – spatiotemporal variability of mainstem CO₂ fluxes**

207 Results from control simulations showed large seasonal ($-0.15 \pm 0.92 \text{ molC m}^{-2} \text{ yr}^{-1}$) and
208 interannual ($-0.15 \pm 0.24 \text{ molC m}^{-2} \text{ yr}^{-1}$) variations in the air-water CO₂ fluxes (Fig. 2). The
209 mainstem Bay was typically estimated to be a net CO₂ sink to the atmosphere during spring and
210 winter when tributary inflows were high, and it shifted to a net CO₂ source in summer and fall.
211 The CO₂ fluxes were comparably less variable on the annual scale, and their magnitude and

212 direction were highly related to the hydrological dry-wet condition. In the dry years (e.g.,
213 1999-2002), the mainstem was estimated a weak CO₂ source or neutral to the atmosphere (with
214 an average efflux of 0.073 molC m⁻² yr⁻¹), which is lower than the efflux derived from bay-wide
215 cruises in the dry 2016 (i.e., 0.73 molC m⁻² yr⁻¹, Chen et al., 2020). In contrast, the mainstem
216 Bay turned into a net CO₂ sink (with an average influx of -0.28 molC m⁻² yr⁻¹) in wet years (e.g.,
217 1996-1997, 2004-2005). Overall, the mainstem was a net CO₂ sink (with an annual average of
218 -0.15 ± 0.24 molC m⁻² yr⁻¹) when averaged over 1996-2005.

219 The CO₂ fluxes showed clear spatial heterogeneity along the mainstem Bay (Fig. 3a). The
220 upper Bay was consistently a strong CO₂ source during the 10-year period, and the efflux was
221 even larger during the wet years, reaching 2.92 molC m⁻² yr⁻¹. In contrast, there were consistent
222 CO₂ influxes in the mid Bay on annual scales, and the average influx was estimated as -0.32
223 molC m⁻² yr⁻¹. The lower Bay simulations showed high interannual variability, where the
224 direction of CO₂ fluxes (i.e., sinks/sources) was greatly influenced by the wet-dry cycles, and
225 this region was primarily a weak CO₂ source in dry years but switched to a net CO₂ sink in wet
226 years.

227 We compared the Susquehanna River flow and CO₂ fluxes in the mainstem Bay to
228 examine their relationships (Fig. 3b). High correlations were found between the two metrics (r
229 $= 0.91$, $p < 0.01$) in the upper Bay, where elevated tributary inflows promoted elevated efflux of
230 CO₂ to the atmosphere. The correlation in the lower Bay was also significant ($r = -0.80$, $p <$
231 0.01), as the CO₂ flux transitioned from a weak source at low flows (i.e., dry years) to a sink at
232 high flows (i.e., wet years).

233 Discharge-CO₂ flux correlations for the mid and entire mainstem Bay were not Bay were
234 not as strong as those in the upper and lower Bay (Fig. 3), and were not statistically significant.
235 The inflow-flux correlation in the mid Bay was relatively modest ($r = 0.59$, $p = 0.07$), because
236 the flux and its flow-related trend at this region are complicated due to its interactions with both
237 the upper and lower Bay, which exhibited contrasting air-water CO₂ flux-flow relationships.
238 The relations between the river inflows and CO₂ fluxes in the mainstem mainly resembled the

239 pattern of the lower Bay, but with a milder trend, displaying a weak source in drought periods
240 and shifting to a net sink during wetter periods.

241 To illustrate dry-wet differences in the CO₂ fluxes, we compared the surface water *p*CO₂ of
242 the mainstem in different seasons between the hydrological dry (year 1999) and wet (year 2004)
243 years. The Susquehanna River inflows in 2004 were much higher in all seasons except during
244 winter, when freshwater inputs were comparable between these two years (Fig. 4a). The spatial
245 patterns of surface water *p*CO₂ in both dry and wet years were generally consistent with
246 previous field observations and model simulations (Chen et al., 2020; Friedman et al., 2020;
247 Shen et al., 2019a). Specifically, the upper Bay was primarily supersaturated in *p*CO₂, with its
248 values in the very upper reaching over 1000 ppm (Fig. 4b-c). The *p*CO₂ level in the mid Bay
249 was mostly below the atmospheric level (i.e., 370 ppm), and the lower Bay was nearly balanced
250 with the atmosphere. Compared with the dry year (1999), the upper Bay was much higher in
251 surface water *p*CO₂ in the wet year (2004). *p*CO₂ in mid Bay was relatively lower in 2004, and
252 this low *p*CO₂ area was observed expanding from the mid Bay to the lower Bay. The
253 differences of surface water *p*CO₂ between the two hydrological years were particularly
254 obvious in summer and fall, when tributary inflows varied substantially.

255

256 **3.2. Control simulations – CO₂ flux and trophic status**

257 We examined the variability of net ecosystem metabolism (NEM, i.e., the difference
258 between primary production and total respiration) in the mainstem, and analyzed the
259 correlations between NEM and air-water CO₂ fluxes. Despite the consistent CO₂ effluxes
260 modeled in the upper Bay, our model identified the upper Bay as heterotrophic (i.e., primary
261 production < total respiration) in wet years but autotrophic (primary production > total
262 respiration) in dry years (Fig. 5a). The upper-Bay NEM in wet years was highly heterotrophic,
263 reaching -10.95 molC m⁻² yr⁻¹. The annual NEM of mid Bay was consistently positive (with an
264 average estimate of 3.65 molC m⁻² yr⁻¹) over the 10-year period, displaying an autotrophic
265 status. The trophic status of the lower Bay was exactly opposite of the upper Bay through time,
266 being autotrophic in wet years, but heterotrophic in dry years.

267 The correlations between NEM and air-water fluxes were extremely high in the upper (r =
268 -0.99, $p < 0.01$) and lower Bay (r = -0.93, $p < 0.01$). The efflux in the upper Bay decreased
269 along with the increase of NEM. In other words, the trophic dynamics with transitions from
270 heterotrophy to autotrophy would reduce CO₂ effluxes in the upper Bay (Fig. 5b). Similarly, the
271 increase of NEM in the lower Bay would promote CO₂ influxes, or reverse the direction from
272 effluxes to influxes of lower-Bay estuarine waters. The mid Bay was principally identified with
273 CO₂ influxes and autotrophy, but no clear correlations were observed between these two
274 metrics in the mid Bay. Overall, an intensified autotrophic status would increase the CO₂ influx
275 in the mainstem Chesapeake Bay.

276

277 **3.3. Sensitivity simulations - impacts of nutrient and OM loading**

278 We examined the relationships between tributary influxes and air-water CO₂ fluxes for
279 different scenarios to distinguish the impacts of riverine nutrient and OM inputs from those of
280 riverine CO₂ inputs and physical mixing processes. CO₂ fluxes between the Control and RiverN
281 (i.e., constant riverine nutrient inputs) scenarios did not differ much in the upper Bay (Fig. 6a),
282 indicating that nutrient input variations associated with the hydrological conditions have little
283 impacts on CO₂ fluxes of the upper Bay. Results of the RiverC (i.e., constant riverine OM
284 inputs) scenario were much different, and the CO₂ fluxes of RiverC scenario did not co-vary
285 significantly with tributary inflows when OM inputs were constant (Fig. 6), indicating that
286 interannual variations in OM inputs regulate variability of upper-Bay CO₂ fluxes. A
287 Comparison between the three scenarios in the lower Bay showed exactly the opposite impacts
288 of riverine nutrient and OM loading as those in the upper Bay (Fig. 6c). The fluxes between the
289 Control and RiverC scenarios in different hydrological years were approximately identical,
290 demonstrating tributary OM loading did not affect the CO₂ flux in the lower Bay. However, the
291 best fit line for RiverN scenario indicated that the CO₂ flux became much less dependent on
292 riverine flows when nutrient inputs did not vary, suggesting that variability of CO₂ fluxes in the
293 lower Bay was more associated with the changes of nutrient inputs.

294 Unlike the upper and lower Bay, both riverine nutrient and OM inputs were found to alter
295 mid-Bay CO₂ fluxes significantly (Fig. 6b). For the RiverN scenario, increases of tributary
296 inflows also lead to reduced influx like the Control Run, however, the air-water flux became
297 more sensitive to the changes of tributary inflows. For RiverC scenario, the trend became
298 different in that higher flows would result in more influxes into the mid Bay. Both riverine
299 nutrient-enhanced production and OM-enhanced respiration were important in the mid Bay,
300 and the best fit lines for CO₂ flux trends suggested overall higher impacts of nutrient inputs (as
301 revealed from the slope differences). Similar to the mid Bay, nutrient and OM inputs both had
302 large impacts on fluxes of mainstem as a whole. Assuming a constant nutrient loading (i.e.,
303 RiverN), the influx magnitude decreased quickly with the increasing of riverine flows, which is
304 opposite to the Control Run (Fig. 6d). The slope change (0.75×10^{-3}) of fit lines between Control
305 and RiverN scenarios was larger than that (0.41×10^{-3}) between Control and RiverC scenario,
306 indicating a more important role of nutrient inputs than OM inputs to mainstem CO₂ flux
307 variations in dry-wet cycles.

308

309 **4. Discussions**

310 **4.1. Spatial variability of air-water CO₂ fluxes**

311 Our results showed distinct features of air-water fluxes for different regions of the
312 mainstem Bay. The upper-Bay surface water was high in $p\text{CO}_2$, and was identified as a net CO₂
313 source to the atmosphere. The overall $p\text{CO}_2$ was below the atmospheric level for mid-Bay
314 waters, and CO₂ sinks during the study period were consistently observed in this region. The
315 lower Bay, however, primarily displayed a neutral condition with shift between sinks and
316 sources associated with hydrological variations. The Susquehanna River water has high $p\text{CO}_2$
317 year-round (supersaturated in most time, Shen et al., 2020), and the riverine freshwater flushes
318 into the upper Bay, where riverine waters directly mix with the upper-Bay estuarine water. In
319 addition to physical mixing, primary production in the upper Bay is largely inhibited due to
320 high turbidity (Xu et al., 2005). Both water column and sediment respiration are fueled by
321 riverine organic supplies (Kemp et al., 1997), leading to substantial DIC generation and CO₂

322 emissions to the air. Water clarity increases significantly in the mid Bay (Testa et al., 2019), and
323 the associated relaxation of light limitation of phytoplankton photosynthesis in the mid Bay
324 leads to autotrophy. The mid Bay is generally higher than the lower or upper Bay in terms of
325 *Chl-a* and productivity, particularly during spring and summer (Harding et al., 2002), which
326 assimilates large amount of DIC and reduces surface water $p\text{CO}_2$ (Xiao et al., 2022). The lower
327 Bay is primarily nutrient limited, and primary production is relatively modest (Zhang et al.,
328 2021; Acker et al., 2005), resulting in a nearly neutral metabolism. Meanwhile, the lower Bay is
329 primarily ocean-dominated, and is influenced by the intrusion of coastal waters with $p\text{CO}_2$
330 close to the atmospheric level. Our study showed the mainstem Bay as a whole displayed a
331 neutral/weak sink condition, close to the lower Bay. This is because the lower Bay occupies
332 ~53% of the total mainstem area (11% and 36% for upper and mid Bay), and the efflux of upper
333 Bay counterbalanced the influx of mid Bay to some extent.

334 Borges and Abril (2011) summarized estuarine CO_2 flux on global scale. Most estuaries in
335 their synthesis have a strong CO_2 efflux to the atmosphere, and are heterotrophic. The global
336 mean CO_2 efflux is $\sim 26 \text{ molC m}^{-2} \text{ yr}^{-1}$. We note that CO_2 effluxes in large estuaries such as the
337 Chesapeake Bay (Herrmann et al., 2020) and Delaware Bay (Joeseof et al., 2015) are orders of
338 magnitude lower. While it is not clear whether adding large estuaries will change the global
339 mean estuarine CO_2 efflux, we suggest this new knowledge need be considered in global
340 estuarine CO_2 flux synthesis. We also wish to point out the bimodal nature of CO_2 flux in large
341 estuaries. Taking the Chesapeake Bay as an example, it is clear the Bay is neither
342 river-dominated nor ocean-dominated. Interestingly, the upper Bay has all the physical,
343 biogeochemical, and CO_2 chemistry features of small river-dominated estuaries reported in the
344 European (Borges et al. 2006; Borges and Abril 2011) and the southeast U.S. (Cai and Wang,
345 1998; Jiang et al. 2008). In contrast, the lower Bay acts as an ocean-dominated estuary in its
346 physical, biogeochemical, and CO_2 chemistry features.

347

348 **4.2. Impacts of hydrological variations on CO_2 fluxes**

349 The hydrological conditions had clear effects on the mainstem air-water CO₂ exchanges
350 during 1996-2005. The magnitude of CO₂ efflux and influx in the upper and mid Bay varied
351 notably between different hydrological years, and the CO₂ flux in the lower Bay even changed
352 the direction during the dry-wet cycles (Fig. 3). During high-flow years, the Susquehanna River
353 dominates the circulation in the upper Bay with its tidal reaches extending into the upper region
354 of mid Bay in some seasons (e.g., spring, Li and Zhong, 2009). Correspondingly, the upper-Bay
355 pCO₂ would be extensively regulated by the riverine-estuarine-water mixing, and displaying a
356 strong CO₂ source in wet years, as revealed from our simulations (Figs. 3-4).

357 The high inflows in wet years are often associated with high nutrient and OM inputs,
358 however, the external nutrient and OM inputs generally lead to opposing effects on inorganic
359 carbon dynamics and air-water CO₂ fluxes. Enhanced photosynthesis/respiration due to
360 external nutrient/OM loading would absorb/release more DIC, thereby decreasing/increasing
361 surface water pCO₂. One may view the inorganic nutrient input as autotrophic loading and the
362 OM input as heterotrophic loading (Cai et al., 2011). Our sensitivity scenarios suggested that
363 riverine OM inputs are the primary driver of CO₂ efflux in the upper Bay (Fig. 6a), indicating
364 that reductions in OM loading would lead to a reduced estuarine CO₂ efflux, and that
365 respiration would be enhanced in wet years. This region is less sensitive to nutrient inputs
366 because the upper Bay is consistently light limited and thus primary production is low,
367 especially in years of high flow when turbidity is much higher. The impacts of riverine nutrient
368 and OM inputs on lower-Bay fluxes were the opposite, where OM inputs from the Susquehanna
369 River were oxidized before reaching the lower Bay, and had little impacts on the total
370 respiration of the lower Bay. In contrast, because high flows transport more nutrients to the
371 lower Bay to stimulate the primary production, the flow-CO₂ flux relationship was weaker in
372 the simulations where nutrient loads were effectively muted with higher flows. Both
373 remotely-sensed and field data revealed a much higher phytoplankton biomass in the lower Bay
374 during high flow years (Acker et al., 2005; Harding et al., 2016), although some of the
375 phytoplankton biomass in the lower Bay might be advected from the productive mid-Bay
376 region rather than locally produced. The mid Bay connects the upper and lower Bay, and

377 variations of nutrient and organic inputs both altered the CO₂ flux. In dry years, the impacts of
378 elevating nutrient loading to a 10-year average level (as revealed from the differences among
379 three scenarios in low-flow dry years, Fig. 6b) would exceed those due to the OM increase,
380 indicating the productive mid Bay is nutrient limited in dry periods. Unlike the dry years, CO₂
381 fluxes in wet years were not sensitive to nutrient load variations, and riverine OM has more
382 influence on the CO₂ flux. From a perspective of 10-year period, the nutrient loading, rather
383 than OM loading, along with tributary inflows was the dominant factor in altering the mid-Bay
384 flux during the hydrological cycle. Similarly, it is the nutrient inputs that contributed to the high
385 correlations between the riverine discharges and air-water CO₂ flux, though OM loading was
386 also an important factor. This is primarily consistent with other large estuarine systems like the
387 Pearl River Estuary (Dai et al., 2008), the Yangtze River Estuary (Chen et al., 2012), and the
388 Mississippi River plume and northern Gulf of Mexico (Huang et al. 2015) that increases of
389 nutrients inputs associated with high flows would increase the influx or shifts from a net source
390 of CO₂ to a net sink of atmospheric CO₂.

391

392 **4.3. Incorporation of estuarine hydrology in CO₂ flux estimates**

393 The CO₂ fluxes showed much variability for the mainstem during the 10 years with large
394 dry-wet cycles. The annual efflux ranged from 0.55 to 2.74 molC m⁻² yr⁻¹ in the upper Bay,
395 from -0.71 to 0.09 molC m⁻² yr⁻¹ in the mid Bay and -1.35 to 0.53 molC m⁻² yr⁻¹ in the lower Bay.
396 The mainstem was estimated to have an annual flux between -0.53 and 0.20 molC m⁻² yr⁻¹. The
397 hydrological impacts on estuarine CO₂ fluxes are mainly associated with the variability in
398 freshwater-estuarine water mixing and estuarine ecosystem metabolism. Borges et al. (2006)
399 implied that a positive NEM is often associated to the CO₂ influx for estuarine waters while a
400 negative NEM is related to an efflux of CO₂, but there is a quantitative disagreement between
401 the intensity of NEM and air-water CO₂ fluxes. The disagreement is probably related to the
402 water residence time. Systems with short water residence time (e.g., the Palma Bay, Spain; the
403 Altamaha Sound, USA) would flush water mass rapidly and the biological activity will have
404 very limited effects on air-water exchanges, however, long water residence systems (e.g., the

405 Scheldt estuary, Belgium-Netherlands; the York River, USA) would accumulate large amounts
406 of DIC through multiple biogeochemical processes and the ventilation of riverine CO₂ has been
407 estimated to contribute to a low portion of overall CO₂ emissions (Jiang et al., 2008; Gazeau et
408 al., 2005). Here we introduced a non-dimensional number (λ), which is the ratio of organic
409 carbon turnover time to the water residence time for the mainstem Chesapeake Bay. The
410 residence time was estimated using the empirical equation from Du and Shen (2016), which
411 relates the water residence time with the mean annual flow of the Susquehanna River.
412 The organic carbon turnover time was calculated with the water-column organic carbon pool
413 divided by NEM from our model. Our study suggested that the wetter periods were
414 characterized by lower λ (Fig. 7), and the variability of mainstem CO₂ fluxes can be well
415 represented using a generic function of λ as confirmed from the high linear correlation ($r = 0.82$)
416 between the two metrics. Water residence time decreased in wet years, however, the reduction
417 of organic carbon turnover time was even faster (due to high NEM), leading to a lower λ and
418 enhanced CO₂ influx for the mainstem Chesapeake Bay. The correlations between λ and
419 air-water exchanges also indicated that nutrient loading is more important in regulating the
420 mainstem CO₂ fluxes compared with the organic matter inputs and ventilation of riverine CO₂.

421 Estuaries and coastal regions are important systems worldwide influencing regional and
422 global carbon cycling. Attempts to assess estuarine and coastal carbon fluxes requires a full
423 incorporation of estuarine hydrology, which brings much uncertainty to air-water exchanges as
424 revealed in this study. Although the controlling mechanism of estuarine CO₂ fluxes associated
425 with the hydrological cycle has not been thoroughly explored, the hydrological impacts has
426 been frequently observed. The four-year dataset over various hydrological conditions in
427 subtropical estuaries of Gulf of Mexico revealed as much as 2-10 times increase in air-water
428 fluxes driven by floods compared with dry periods (Yao et al., 2022). Similarly, CO₂ emissions
429 from the Pearl River Estuary in wet periods was estimated as ~6 times of that in dry periods
430 (Guo et al., 2009). The New River Estuary in the East Coast of U.S. was highly impacted from
431 freshwater inflows that the estuarine system was estimated to be a weak CO₂ sink in a dry year,
432 but shifted to a moderate source in the consecutive wet year (Crosswell et al., 2017). Hence, the

433 global carbon budget estimates need to fully consider the interannual variability of air-water
434 fluxes, particularly in estuarine and coastal environments, where short-term estimates of
435 air-water fluxes could be highly biased, and should be carefully used to interpolate into much
436 larger spatiotemporal scales.

437

438 **4.4. Other factors that influence interannual CO₂ fluxes**

439 In this study, we examined the hydrological controls on estuarine CO₂ flux by investigating
440 the variability of CO₂ flux due to riverine nutrient and OM inputs, which have very different
441 impacts on CO₂ cycling and are tightly associated with hydrological conditions. However, there
442 are other factors that relate to the hydrological conditions and may also alter air-water fluxes
443 significantly and could be the focus of future studies. For example, high tributary inflows
444 generally lead to elevated suspended sediments in estuarine waters, either by directly increasing
445 external loading of riverine particles or by enhancing scouring of bottom sediments with
446 comparably higher near-bottom currents. Historical data suggested that high flow generally
447 produced very turbid conditions (with high light attenuation coefficients) in the upper Bay
448 (Harding et al., 1994). The changes of light conditions in different hydrological years would
449 inevitably alter bay-wide primary production and affect the air-water exchanges. The
450 Chesapeake Bay is experiencing rapid climate change, and the surface water temperature in the
451 Bay increased at the rate of 0.05 to 0.10 °C yr⁻¹ during the past 30 years (Ni et al., 2020).
452 Although no significant correlations between tributary inflows and bay-wide surface water
453 temperature were observed, the interannual variability of surface water temperature is evident
454 (0.7 °C) between 1996 - 2005. The water temperature variations would directly affect the
455 air-water CO₂ exchanges by regulating CO₂ solubility, surface water pCO₂, and the other
456 important biogeochemical processes.

457

458 **5. Conclusions**

459 In this study, we investigated the hydrological controls on CO₂ fluxes in the mainstem
460 Chesapeake Bay using a coupled physical-biogeochemical model. Our model revealed

461 significant spatiotemporal variability in bay-wide fluxes over the 10-year period. The upper
462 Bay was consistently a net CO₂ source on the annual scale, and the mid Bay was a net sink. The
463 lower Bay shifted from a net source in dry years to a net sink in wet years. The entire mainstem
464 was identified a net sink mostly with exceptions in drought periods, when the mainstem was a
465 net source. Sensitivity scenario results suggested substantial effects of riverine nutrient and OM
466 inputs to CO₂ flux variations. The high correlations between tributary inputs and upper-Bay
467 fluxes were due to enhanced respiration under increased OM inputs. The interannual flux
468 variation in the lower Bay was mostly regulated by nutrient inputs and associated stimulation of
469 primary productivity. Both nutrient and OM inputs contributed to the flux variability in the mid
470 Bay. Our results revealed that the CO₂ flux of the mainstem was more sensitive to tributary
471 nutrient inputs associated with hydrological changes, rather than the import of organic matter or
472 high-*p*CO₂ freshwater.

473

474 **Acknowledgement**

475 This study was funded by the United States National Oceanographic and Atmospheric
476 Administration Ocean Acidification Program (NOAA-OAP; award # NA15NOS4780184).
477 This is UMCES contribution number XXXX.

478

479 **Conflict of Interest**

480 The authors declare no competing financial interest.

481

References

- 482 Acker, J.G., Harding, L.W., Leptoukh, G., Zhu, T. and Shen, S., 2005. Remotely-sensed chl a at the
483 Chesapeake Bay mouth is correlated with annual freshwater flow to Chesapeake Bay. *Geophysical*
484 *Research Letters*, 32(5).
- 485 Abril, G. and Borges, A.V., 2005. Carbon dioxide and methane emissions from estuaries. In *Greenhouse*
486 *gas emissions—fluxes and processes* (pp. 187-207). Springer, Berlin, Heidelberg.
- 487 Borges, A.V., Schiettecatte, L.S., Abril, G., Delille, B. and Gazeau, F., 2006. Carbon dioxide in
488 European coastal waters. *Estuarine, Coastal and Shelf Science*, 70(3), pp.375-387.
- 489 Borges, A.V., Delille, B. and Frankignoulle, M., 2005. Budgeting sinks and sources of CO₂ in the coastal
490 ocean: Diversity of ecosystems counts. *Geophysical research letters*, 32(14).

491 Borges, A. V, and G. Abril. 2011. 5.04 - Carbon dioxide and methane dynamics in estuaries, p. 119–
492 161. In W. Editors-in-Chief: Eric and M. Donald [eds.], *Treatise on Estuarine and Coastal Science*.
493 Academic Press.

494 Caffrey, J.M., 2004. Factors controlling net ecosystem metabolism in US estuaries. *Estuaries*, 27(1),
495 pp.90-101.

496 Cai, W.J. and Wang, Y., 1998. The chemistry, fluxes, and sources of carbon dioxide in the estuarine
497 waters of the Satilla and Altamaha Rivers, Georgia. *Limnology and Oceanography*, 43(4),
498 pp.657-668.

499 Cai, W.J., 2011. Estuarine and coastal ocean carbon paradox: CO₂ sinks or sites of terrestrial carbon
500 incineration?. *Annual review of marine science*, 3, pp.123-145.

501 Chen, B., Cai, W.J., Brodeur, J.R., Hussain, N., Testa, J.M., Ni, W. and Li, Q., 2020. Seasonal and spatial
502 variability in surface p CO₂ and air–water CO₂ flux in the Chesapeake Bay. *Limnology and*
503 *Oceanography*, 65(12), pp.3046-3065.

504 Chen, C.T.A., Huang, T.H., Fu, Y.H., Bai, Y. and He, X., 2012. Strong sources of CO₂ in upper estuaries
505 become sinks of CO₂ in large river plumes. *Current Opinion in Environmental Sustainability*, 4(2),
506 pp.179-185.

507 Cotovicz Jr, L.C., Knoppers, B.A., Brandini, N., Costa Santos, S.J. and Abril, G., 2015. A strong CO₂
508 sink enhanced by eutrophication in a tropical coastal embayment (Guanabara Bay, Rio de Janeiro,
509 Brazil). *Biogeosciences*, 12(20), pp.6125-6146.

510 Crosswell, J.R., Wetz, M.S., Hales, B. and Paerl, H.W., 2012. Air-water CO₂ fluxes in the microtidal
511 Neuse River estuary, North Carolina. *Journal of Geophysical Research: Oceans*, 117(C8).

512 Crosswell, J.R., Anderson, I.C., Stanhope, J.W., Van Dam, B., Brush, M.J., Ensign, S., Piehler, M.F.,
513 McKee, B., Bost, M. and Paerl, H.W., 2017. Carbon budget of a shallow, lagoonal estuary:
514 Transformations and source-sink dynamics along the river-estuary-ocean continuum. *Limnology*
515 *and Oceanography*, 62(S1), pp.S29-S45.

516 Dai, M., Zhai, W., Cai, W.J., Callahan, J., Huang, B., Shang, S., Huang, T., Li, X., Lu, Z., Chen, W. and
517 Chen, Z., 2008. Effects of an estuarine plume-associated bloom on the carbonate system in the
518 lower reaches of the Pearl River estuary and the coastal zone of the northern South China
519 Sea. *Continental Shelf Research*, 28(12), pp.1416-1423.

520 Dinauer, A. and Mucci, A., 2017. Spatial variability in surface-water pCO₂ and gas exchange in the
521 world's largest semi-enclosed estuarine system: St. Lawrence Estuary
522 (Canada). *Biogeosciences*, 14(13), pp.3221-3237.

523 Du, J. and Shen, J., 2016. Water residence time in Chesapeake Bay for 1980–2012. *Journal of Marine*
524 *Systems*, 164, pp.101-111.

525 Friedman, J.R., Shadwick, E.H., Friedrichs, M.A., Najjar, R.G., De Meo, O.A., Da, F. and Smith, J.L.,
526 2020. Seasonal variability of the CO₂ system in a large coastal plain estuary. *Journal of*
527 *Geophysical Research: Oceans*, 125(1), p.e2019JC015609.

528 Gazeau, F., Duarte, C.M., Gattuso, J.P., Barrón, C., Navarro, N., Ruiz, S., Prairie, Y.T., Calleja, M.,
529 Delille, B., Frankignoulle, M. and Borges, A.V., 2005. Whole-system metabolism and CO₂ fluxes
530 in a Mediterranean Bay dominated by seagrass beds. *Biogeosciences*, 2(1), pp.43-60.

531 Guo, X., Cai, W.-J., Huang, W.-J., Wang, Y., Chen, F., Murrell, M.C., Lohrenz, S. Dai, M., Jiang, L.-Q.
532 and Culp, R., 2012. CO₂ dynamics and community metabolism in the Mississippi River plume.
533 *Limnology and Oceanography* 57(1):1-17.

534 Gypens, N., Borges, A.V. and Lancelot, C., 2009. Effect of eutrophication on air–sea CO₂ fluxes in the
535 coastal Southern North Sea: a model study of the past 50 years. *Global Change Biology*, 15(4),
536 pp.1040-1056.

537 Harding, L.W., 1994. Long-term trends in the distribution of phytoplankton in Chesapeake Bay: roles of
538 light, nutrients and streamflow. *Marine Ecology-Progress Series*, 104, pp.267-267.

539 Harding Jr, L.W., Mallonee, M.E. and Perry, E.S., 2002. Toward a predictive understanding of primary
540 productivity in a temperate, partially stratified estuary. *Estuarine, Coastal and Shelf Science*, 55(3),
541 pp.437-463.

542 Harding, L.W., Gallegos, C.L., Perry, E.S., Miller, W.D., Adolf, J.E., Mallonee, M.E. and Paerl, H.W.,
543 2016. Long-term trends of nutrients and phytoplankton in Chesapeake Bay. *Estuaries and*
544 *Coasts*, 39(3), pp.664-681.

545 Herrmann, M., Najjar, R.G., Da, F., Friedman, J.R., Friedrichs, M.A., Goldberger, S., Menendez, A.,
546 Shadwick, E.H., Stets, E.G. and St-Laurent, P., 2020. Challenges in quantifying air-water carbon
547 dioxide flux using estuarine water quality data: Case study for Chesapeake Bay. *Journal of*
548 *Geophysical Research: Oceans*, 125(7), p.e2019JC015610.

549 Huang, W.-J., Cai, W.-J., Wang, Y., Hu, X., Chen, B., Lohrenz, S.E., Chakraborty, S., He, R., Brandes, J.,
550 Hopkinson, C.S., 2015. The response of inorganic carbon distributions and dynamics to
551 upwelling-favorable winds on the northern Gulf of Mexico during summer. *Cont. Shelf Res.* 111,
552 211–222. doi:10.1016/j.csr.2015.08.020

553 Jiang, L.Q., Cai, W.J. and Wang, Y., 2008. A comparative study of carbon dioxide degassing in river-
554 and marine-dominated estuaries. *Limnology and Oceanography*, 53(6), pp.2603-2615.

555 Joesoef, A., Huang, W.J., Gao, Y. and Cai, W.J., 2015. Air–water fluxes and sources of carbon dioxide
556 in the Delaware Estuary: spatial and seasonal variability. *Biogeosciences*, 12(20), pp.6085-6101.

557 Joesoef, A., Kirchman, D.L., Sommerfield, C.K. and Cai, W.J., 2017. Seasonal variability of the
558 inorganic carbon system in a large coastal plain estuary. *Biogeosciences*, 14(21), pp.4949-4963.

559 Kemp, W.M., Smith, E.M., Marvin-DiPasquale, M. and Boynton, W.R., 1997. Organic carbon balance
560 and net ecosystem metabolism in Chesapeake Bay. *Marine Ecology Progress Series*, 150,
561 pp.229-248.

562 Laruelle, G.G., Dürr, H.H., Slomp, C.P. and Borges, A.V., 2010. Evaluation of sinks and sources of CO₂
563 in the global coastal ocean using a spatially-explicit typology of estuaries and continental
564 shelves. *Geophysical Research Letters*, 37(15).

565 Li, M., Zhong, L. and Boicourt, W.C., 2005. Simulations of Chesapeake Bay estuary: Sensitivity to
566 turbulence mixing parameterizations and comparison with observations. *Journal of Geophysical*
567 *Research: Oceans*, 110(C12).

568 Li, M., Lee, Y.J., Testa, J.M., Li, Y., Ni, W., Kemp, W.M. and Di Toro, D.M., 2016. What drives
569 interannual variability of hypoxia in Chesapeake Bay: Climate forcing versus nutrient
570 loading?. *Geophysical Research Letters*, 43(5), pp.2127-2134.

571 Li, M. and Zhong, L., 2009. Flood–ebb and spring–neap variations of mixing, stratification and
572 circulation in Chesapeake Bay. *Continental Shelf Research*, 29(1), pp.4-14.

573 Li, M., Li, R., Cai, W.J., Testa, J.M. and Shen, C., 2020. Effects of wind-driven lateral upwelling on
574 estuarine carbonate chemistry. *Frontiers in Marine Science*, 7, p.588465.

575 Li, M., Guo, Y., Cai, W.J., Testa, J.M., Shen, C., Li, R. and Su, J., 2023. Projected increase in carbon
576 dioxide drawdown and acidification in large estuaries under climate change. *Communications*
577 *Earth & Environment*, 4(1), p.68.

578 Magnuson, A., Harding Jr, L.W., Mallonee, M.E. and Adolf, J.E., 2004. Bio-optical model for
579 Chesapeake Bay and the middle Atlantic bight. *Estuarine, Coastal and Shelf Science*, 61(3),
580 pp.403-424.

581 Pacheco, F.S., Soares, M.C.S., Assireu, A.T., Curtarelli, M.P., Roland, F., Abril, G., Stech, J.L., Alvalá,
582 P.C. and Ometto, J.P., 2015. The effects of river inflow and retention time on the spatial
583 heterogeneity of chlorophyll and water–air CO₂ fluxes in a tropical hydropower
584 reservoir. *Biogeosciences*, 12(1), pp.147-162.

585 Regnier, P., Friedlingstein, P., Ciais, P., Mackenzie, F.T., Gruber, N., Janssens, I.A., Laruelle, G.G.,
586 Lauerwald, R., Luysaert, S., Andersson, A.J. and Arndt, S., 2013. Anthropogenic perturbation of
587 the carbon fluxes from land to ocean. *Nature geoscience*, 6(8), pp.597-607.

588 Rosentreter, J.A., Maher, D.T., Erler, D.V., Murray, R. and Eyre, B.D., 2018. Factors controlling
589 seasonal CO₂ and CH₄ emissions in three tropical mangrove-dominated estuaries in
590 Australia. *Estuarine, Coastal and Shelf Science*, 215, pp.69-82.

591 Shen, C., Testa, J.M., Li, M., Cai, W.J., Waldbusser, G.G., Ni, W., Kemp, W.M., Cornwell, J., Chen, B.,
592 Brodeur, J. and Su, J., 2019a. Controls on carbonate system dynamics in a coastal plain estuary: A
593 modeling study. *Journal of Geophysical Research: Biogeosciences*, 124(1), pp.61-78.

594 Shen, C., Testa, J.M., Ni, W., Cai, W.J., Li, M. and Kemp, W.M., 2019b. Ecosystem metabolism and
595 carbon balance in Chesapeake Bay: A 30-year analysis using a coupled hydrodynamic-
596 biogeochemical model. *Journal of Geophysical Research: Oceans*, 124(8), pp.6141-6153.

597 Shen, C., Testa, J.M., Li, M. and Cai, W.J., 2020. Understanding anthropogenic impacts on pH and
598 aragonite saturation state in Chesapeake Bay: Insights from a 30-year model study. *Journal of*
599 *Geophysical Research: Biogeosciences*, 125(7), p.e2019JG005620.

600 St-Laurent, P., Friedrichs, M.A., Najjar, R.G., Shadwick, E.H., Tian, H. and Yao, Y., 2020. Relative
601 impacts of global changes and regional watershed changes on the inorganic carbon balance of the
602 Chesapeake Bay. *Biogeosciences*, 17(14), pp.3779-3796.

603 Testa, J.M., Li, Y., Lee, Y.J., Li, M., Brady, D.C., Di Toro, D.M., Kemp, W.M. and Fitzpatrick, J.J., 2014.
604 Quantifying the effects of nutrient loading on dissolved O₂ cycling and hypoxia in Chesapeake Bay
605 using a coupled hydrodynamic–biogeochemical model. *Journal of Marine Systems*, 139,
606 pp.139-158.

607 Testa, J.M., Lyubchich, V. and Zhang, Q., 2019. Patterns and trends in Secchi disk depth over three
608 decades in the Chesapeake Bay estuarine complex. *Estuaries and Coasts*, 42(4), pp.927-943.

609 Van Dam, B.R., Crosswell, J.R., Anderson, I.C. and Paerl, H.W., 2018. Watershed-scale drivers of air-
610 water CO₂ exchanges in two lagoonal North Carolina (USA) estuaries. *Journal of Geophysical*
611 *Research: Biogeosciences*, 123(1), pp.271-287.

612 Wanninkhof, R. 2014. Relationship between wind speed and gas exchange over the ocean
613 revisited. *Limnology and Oceanography: Methods*, 12(6), pp.351-362.

614 Weiss, R. 1974. Carbon dioxide in water and seawater: The solubility of a non-ideal gas. *Marine*
615 *Chemistry*, 2(3), pp.203-215.

616 Xiao, Q., Xu, X., Duan, H., Qi, T., Qin, B., Lee, X., Hu, Z., Wang, W., Xiao, W. and Zhang, M., 2020.
617 Eutrophic Lake Taihu as a significant CO₂ source during 2000–2015. *Water Research*, 170,
618 p.115331.

619 Xiao, Q., Duan, H., Qin, B., Hu, Z., Zhang, M., Qi, T. and Lee, X., 2022. Eutrophication and temperature
620 drive large variability in carbon dioxide from China's Lake Taihu. *Limnology and*
621 *Oceanography*, 67(2), pp.379-391.

622 Xu, J., Hood, R.R. and Chao, S.Y., 2005. A simple empirical optical model for simulating light
623 attenuation variability in a partially mixed estuary. *Estuaries*, 28(4), pp.572-580

624 Yao, H., McCutcheon, M.R., Staryk, C.J. and Hu, X., 2020. Hydrologic controls on CO₂ chemistry and
625 flux in subtropical lagoonal estuaries of the northwestern Gulf of Mexico. *Limnology and*
626 *Oceanography*, 65(6), pp.1380-1398.

627 Yao, H., Montagna, P.A., Wetz, M.S., Staryk, C.J. and Hu, X., 2022. Subtropical estuarine carbon budget
628 under various hydrologic extremes and implications on the lateral carbon exchange from tidal
629 wetlands. *Water Research*, 217, p.118436.

630 Zhang, Q., Fisher, T.R., Trentacoste, E.M., Buchanan, C., Gustafson, A.B., Karrh, R., Murphy, R.R.,
631 Keisman, J., Wu, C., Tian, R. and Testa, J.M., 2021. Nutrient limitation of phytoplankton in
632 Chesapeake Bay: Development of an empirical approach for water-quality management. *Water*
633 *Research*, 188, p.116407.

634 Zhong, J., Wallin, M.B., Wang, W., Li, S.L., Guo, L., Dong, K., Ellam, R.M., Liu, C.Q. and Xu, S., 2021.
635 Synchronous evaporation and aquatic primary production in tropical river networks. *Water*
636 *Research*, 200, p.117272.

637
638

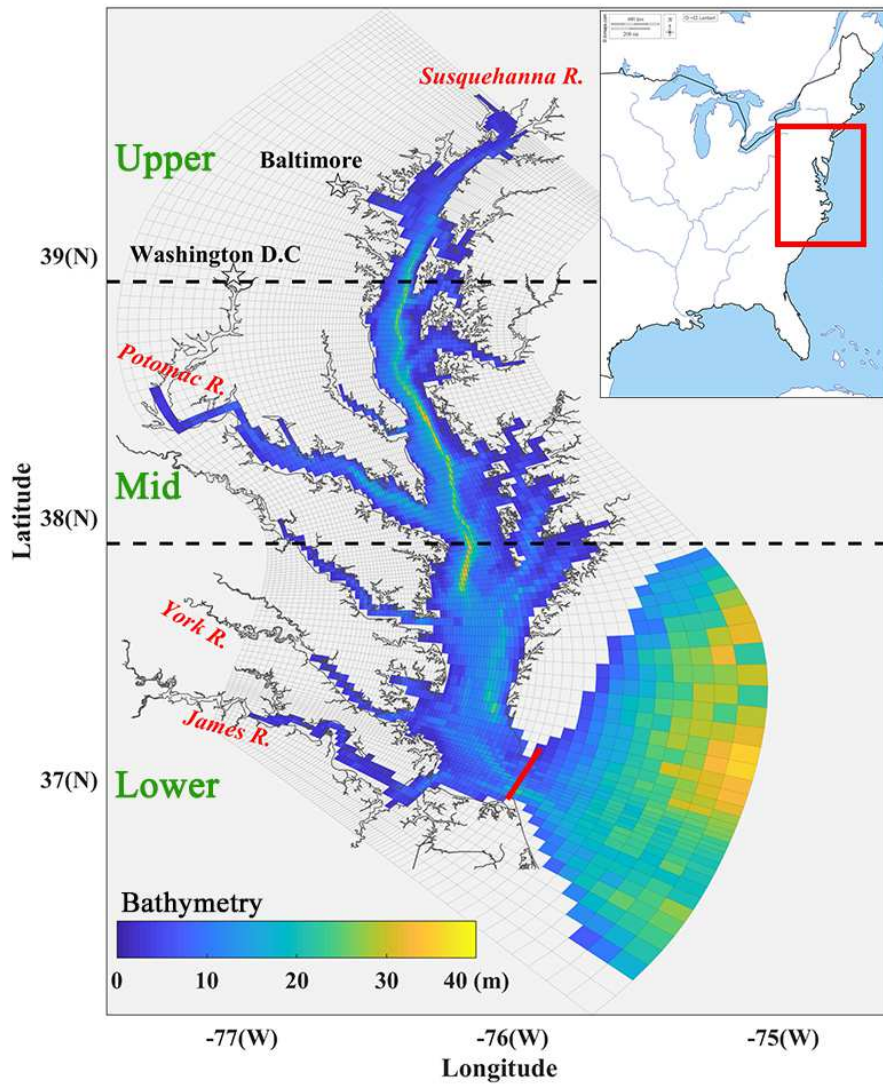


Fig. 1. Map of the Chesapeake Bay, including its regional location, key geographic features, major tributary rivers, the bathymetry, the boundaries between upper, mid and lower Bay, and the mesh grids for model simulations.

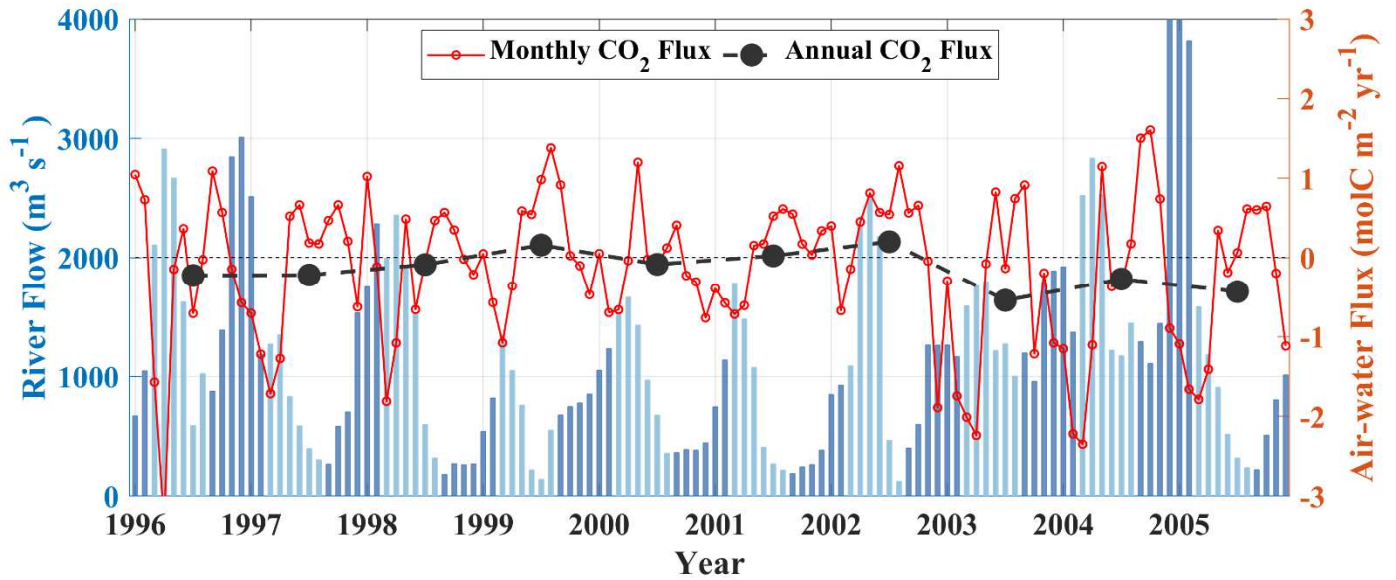


Fig. 2. (Left axis) monthly discharges of the Susquehanna River during 1996-2005. Dark blue represents the winter-spring period, and light blue represents the summer-fall period. (right axis) monthly (red line) and annual (black line) mean CO₂ fluxes of the mainstem Chesapeake Bay during 1996-2005. Positive fluxes (+) represent efflux, and negative fluxes (-) represent influx.

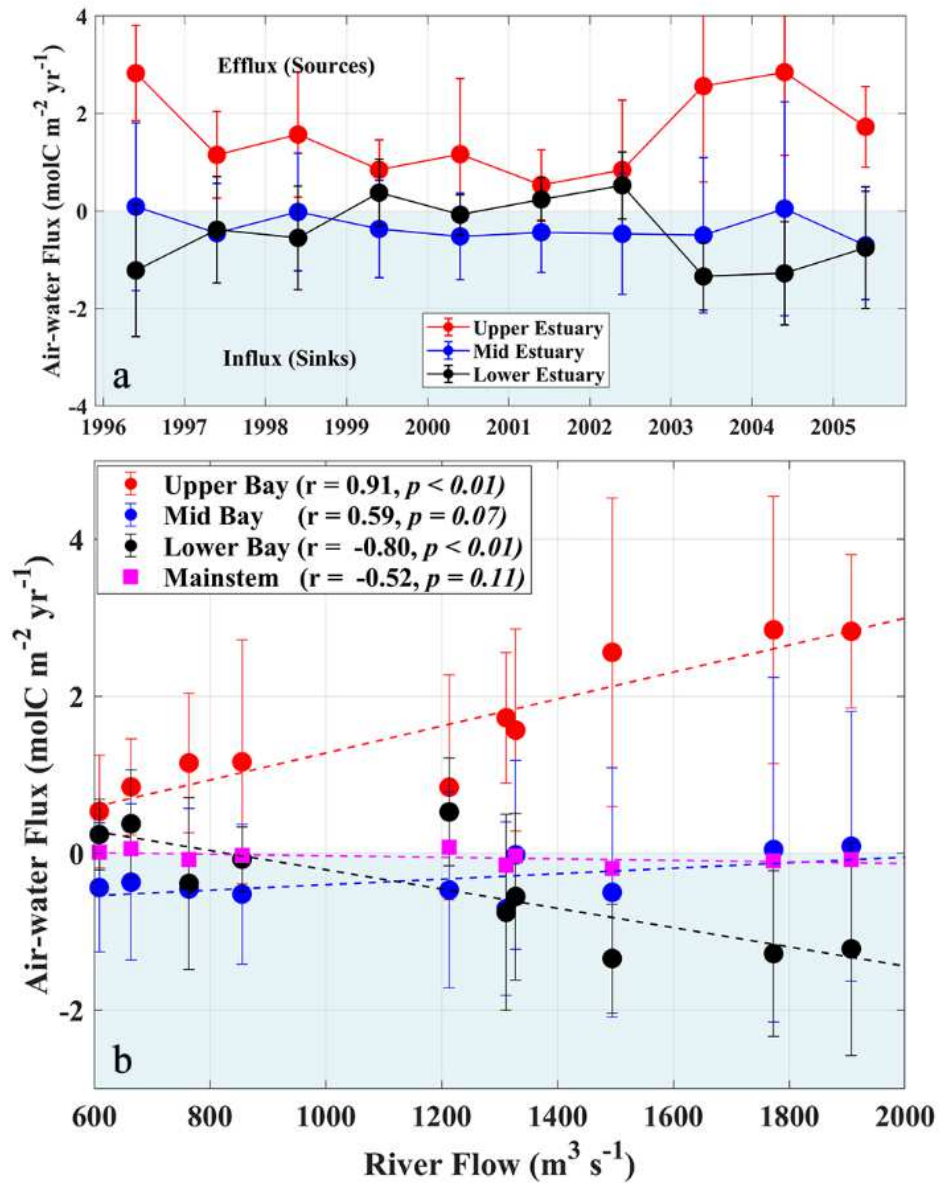


Fig. 3. (a) Model estimated CO₂ fluxes in the upper, mid and lower Bay from 1996 to 2005; (b) comparisons between annual inflows of the Susquehanna River and CO₂ fluxes in the mainstem during the study period. Positive fluxes (+) represent efflux, and negative fluxes (-) represent influx.

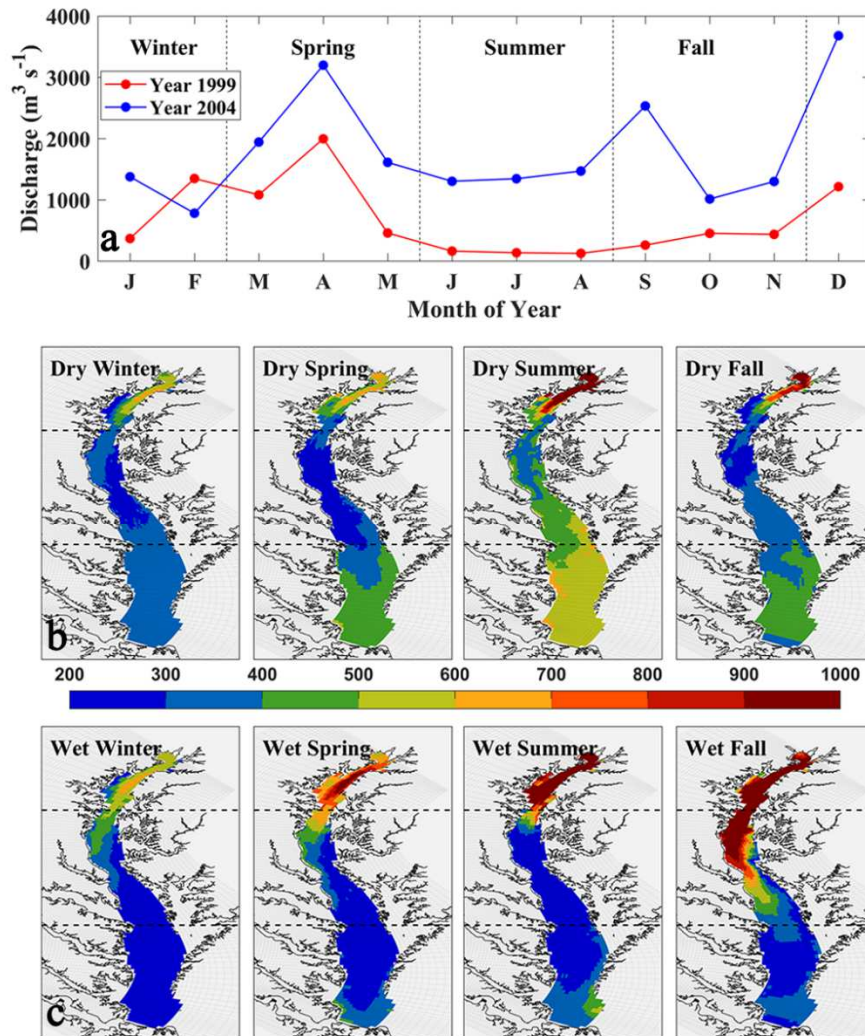


Fig. 4. (a) Monthly Susquehanna River inflows during the dry (1999) and wet (2004) year; seasonally averaged surface water $p\text{CO}_2$ (uatm) during the (b) dry and (c) wet years. The dashed lines are the boundaries of upper, mid and lower Bay.

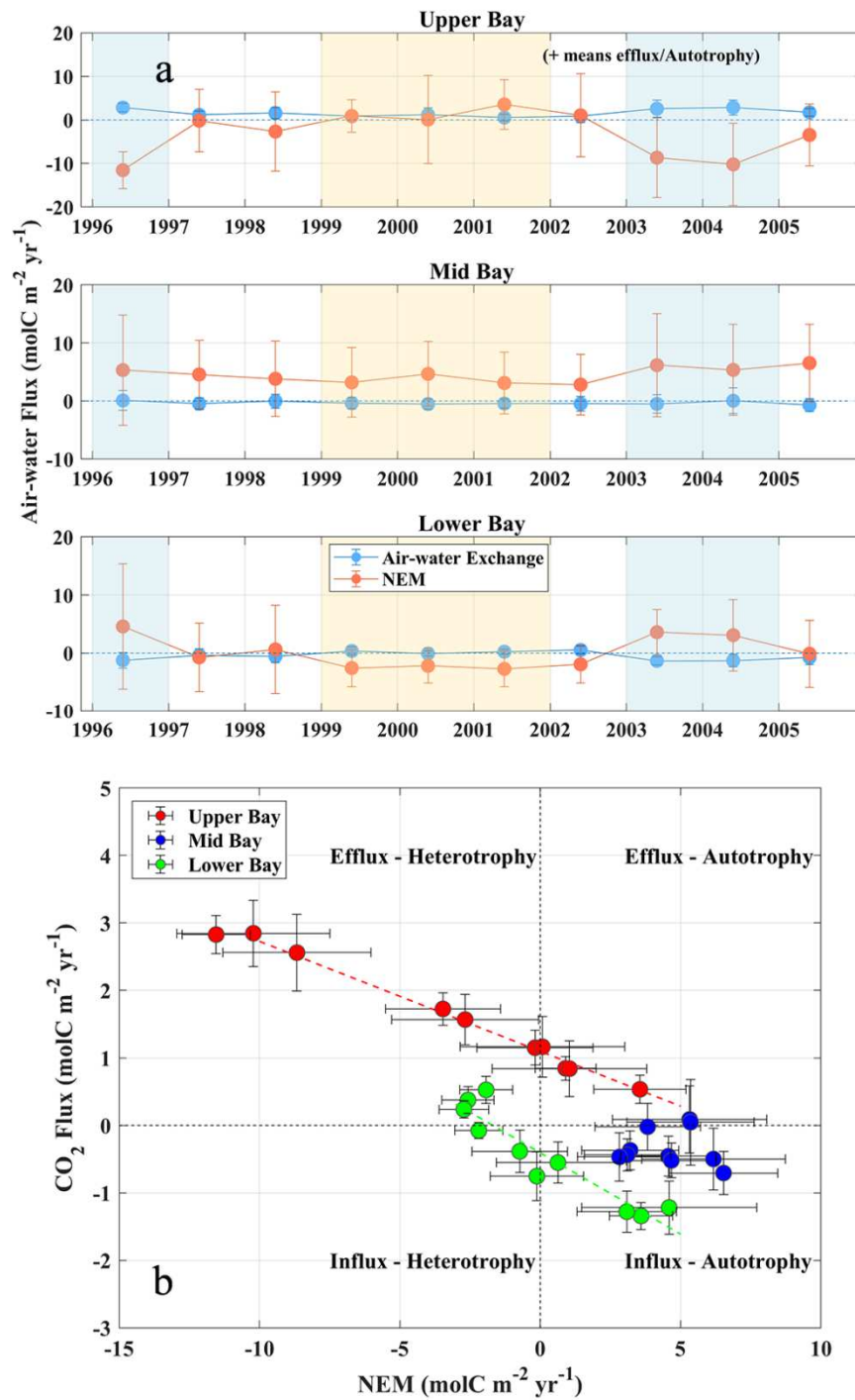


Fig. 5. (a) Comparisons between the annual net ecosystem metabolism (NEM) and CO₂ fluxes in upper, mid and lower Bay during 1996-2005 (light-blue shadow represents wet years, and light-yellow shadow represents dry years.); (b) correlations between NEM and air-water fluxes. The dashed lines are the best fit lines.

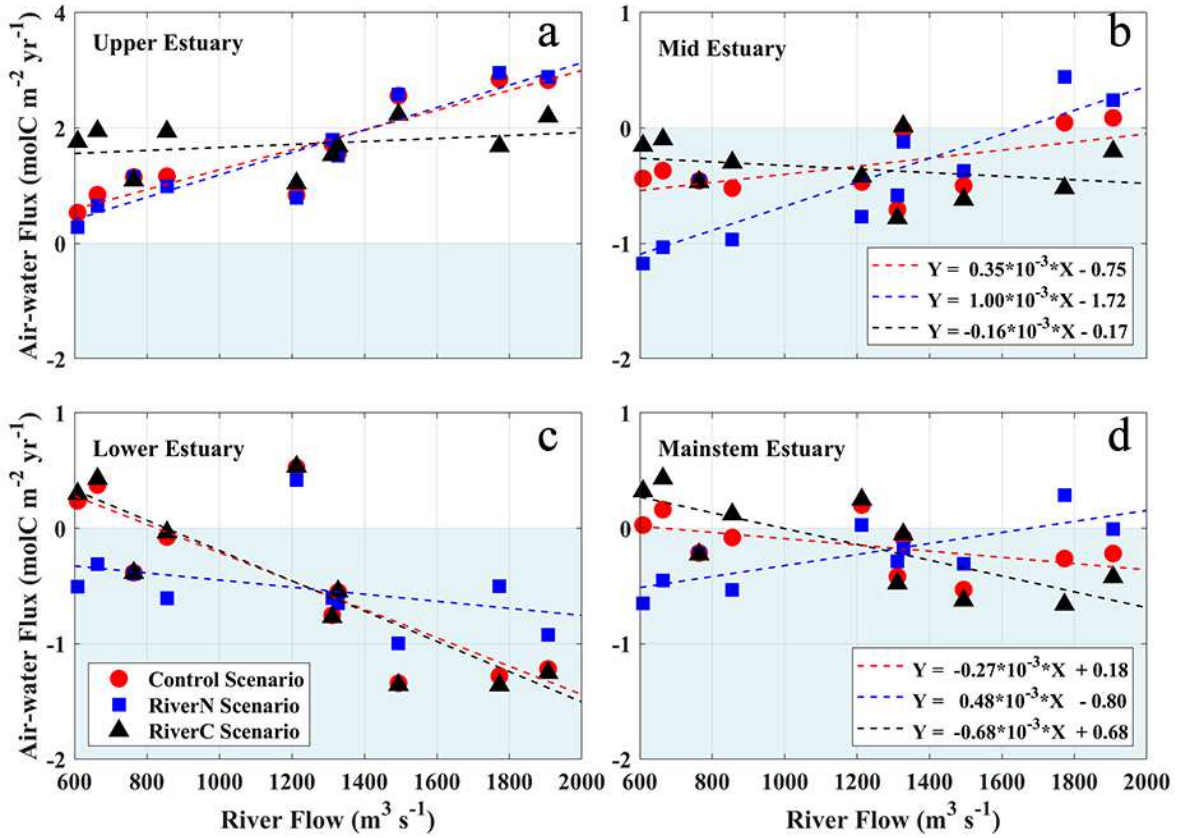


Fig. 6. Comparison between tributary inflows and CO₂ exchanges in the (a) upper, (b) mid, (c) lower and (d) the mainstem Bay for different sensitivity scenarios. Dashed lines are the best fit lines.

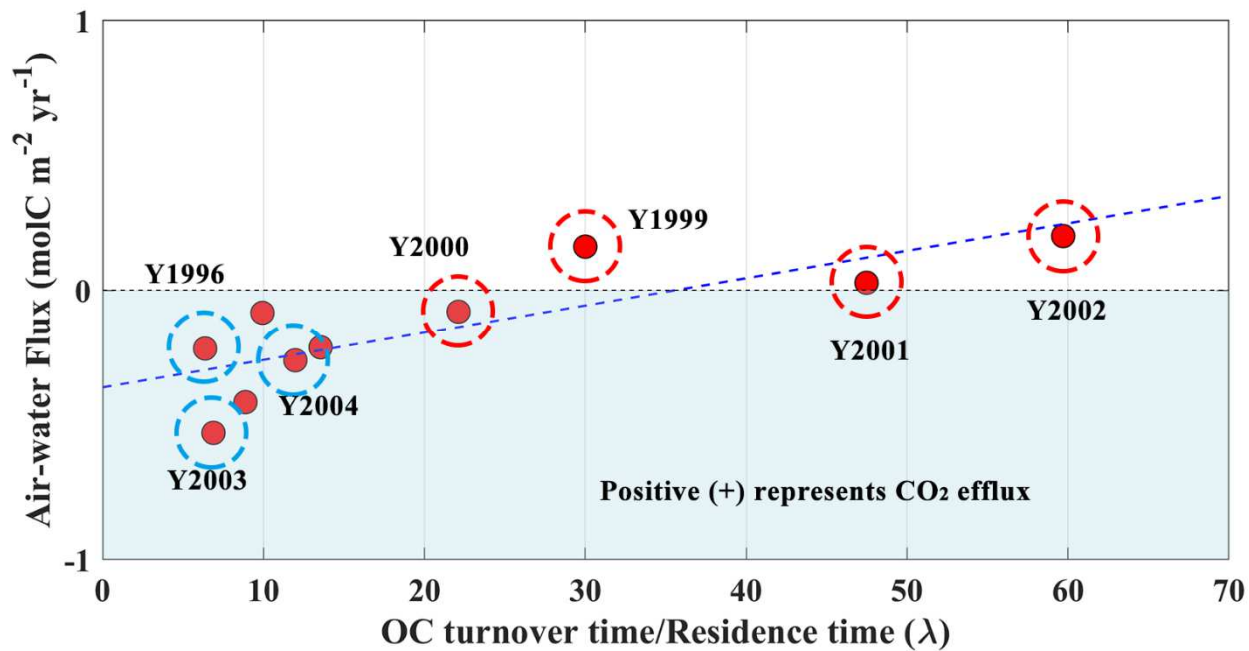


Fig. 7. Comparison between annually averaged air-water fluxes and λ (the ratio of organic carbon turnover time to water residence time) in the mainstem Bay. The dashed line is the best fit line. Red circles represent the dry years, and blue circles represent the wet years.

Graphic Abstract

